Bilayer registry in a multicomponent asymmetric membrane: Dependence on lipid composition and chain length

Anirban Polley,[1] Satyajit Mayor,[2] and Madan Rao[1,2,a)]
[1]*Raman Research Institute, C.V. Raman Avenue, Bangalore 560080, India*
[2]*National Centre for Biological Sciences (TIFR), Bellary Road, Bangalore 560065, India*

(Received 16 April 2014; accepted 23 July 2014; published online 11 August 2014)

A question of considerable interest to cell membrane biology is whether phase segregated domains across an asymmetric bilayer are strongly correlated with each other and whether phase segregation in one leaflet can induce segregation in the other. We answer both these questions in the affirmative, using an atomistic molecular dynamics simulation to study the equilibrium statistical properties of a 3-component *asymmetric* lipid bilayer comprising an unsaturated palmitoyl-oleoyl-phosphatidylcholine, a saturated sphingomyelin, and cholesterol with different composition ratios. Our simulations are done by fixing the composition of the upper leaflet to be at the coexistence of the liquid ordered (l_o)-liquid disordered (l_d) phases, while the composition of the lower leaflet is varied from the phase coexistence regime to the mixed l_d phase, across a first-order phase boundary. In the regime of phase coexistence in each leaflet, we find strong transbilayer correlations of the l_o domains across the two leaflets, resulting in *bilayer registry*. This transbilayer correlation depends sensitively upon the chain length of the participating lipids and possibly other features of lipid chemistry, such as degree of saturation. We find that the l_o domains in the upper leaflet can *induce* phase segregation in the lower leaflet, when the latter is nominally in the mixed (l_d) phase. © *2014 AIP Publishing LLC*. [http://dx.doi.org/10.1063/1.4892087]

I. INTRODUCTION

Cell membranes are composed of many different lipid species and exhibit both lateral heterogeneity[1–3] and bilayer asymmetry in their lipid composition.[4] While there have been many *in vitro* studies of lateral phase segregation in multicomponent giant unilamellar vesicles (GUVs)[5–7] and suspended membranes,[5,6] it is only recently that attention has turned to membranes with asymmetric bilayers.[8,9] One of the issues highlighted in these experiments and relevant to cell membrane biology, is the extent of correlation or registry of phase segregated domains in the two leaflets of the bilayer. This has inspired theoretical[10,11] and coarse-grained computer simulation[12] studies of *bilayer registry* of domains in asymmetric bilayers. A well studied multicomponent model system is the 3-component lipid mixture comprising an unsaturated lipid (POPC), a saturated lipid (PSM), and cholesterol (Chol) which exhibits liquid-ordered (l_o)-liquid-disordered (l_d) phase coexistence. Since the physical characteristics of membrane composition, namely, the extent of bilayer registry, is likely to be sensitive to lipid chemistry, in this paper we study the transbilayer coupling and extent of bilayer registry of the phase domains across the membrane, using an atomistic molecular dynamics (MD) simulation of an asymmetric lipid bilayer membrane comprising POPC/PSM/Chol.

The registry of lipids across the bilayer suggests a mechanism by which outer leaflet lipids may couple with inner leaflet lipids and vice versa. This is important in the construction of membrane domains, and more generally in transducing information across the bilayer by lipidic receptors such as GPI-anchored proteins (GPI-APs)[13] or glycolipids[14] and other lipid species. Our motivation for this work also comes from a series of experiments that study the spatial organization and dynamics of GPI-APs, on the surface of living cells. A variety of experimental strategies such as Fluorescence Resonance Energy Transfer (FRET),[4,15–18] near-field microscopy (NSOM), and electron microscopy, have revealed that both the organization and dynamics of the outer-leaflet GPI-APs are regulated by cholesterol, sphingolipids, and *cortical actin and myosin* at the inner leaflet. The question is how do the outer-leaflet GPI-APs couple to cortical actin that abuts the inner leaflet of the cell membrane.[17,18] Since the interaction across the bilayer must be indirect, are there other lipids, such as cholesterol and sphingolipids, that are involved in this linkage? Do specific inner leaflet lipids that interact with actin, participate in this transbilayer coupling?[18] This naturally brings up the issue of bilayer registry in the cell membrane and its dependence on the specificity of lipids and its chemistry. We have been addressing these important issues using both experiments on live cells and atomistic molecular dynamics simulations on multicomponent model membranes composed of so-called "raft-components."[1]

The article is organized as follows: We first describe the details of the atomistic molecular dynamics simulation of the 3-component bilayer. Next we present our results on lateral compositional heterogeneity, extent of bilayer registry, and mismatch area across the bilayer, as a function of the concentration of the saturated lipid (PSM). We also study how changes in lipid chain length of SM affect bilayer registry. We end with a short summary of the results and conclusions.

a)Electronic addresses: madan@rri.res.in and madan@ncbs.res.in

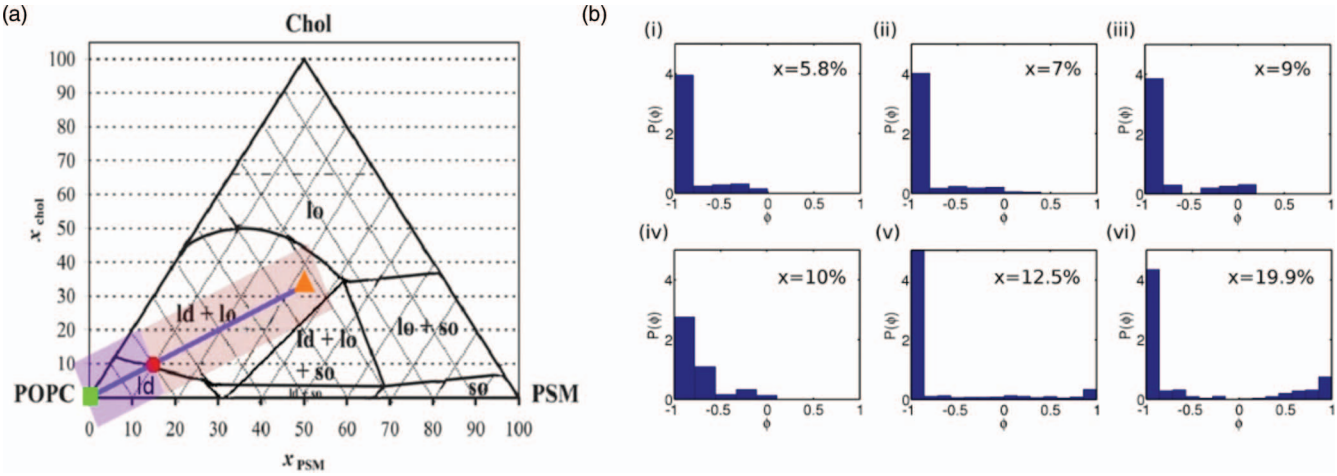

FIG. 1. (a) Ternary phase diagram of POPC, PSM, and CHOL at $T = 23\,^{\circ}$C taken from Ref. 28. Triangle (orange) represents the composition 1 : 1 : 1 which is deep in the phase coexistence region; dot (red) is a point on the phase boundary $x_c = 10\%$. (b) We have verified this phase diagram by doing simulations at different compositions along the blue line in (a). Panel shows the probability distribution of the phase segregation order parameter ϕ (main text) for the symmetric bilayer at different values of x: (i)-(iii) shows that for $x < 10\%$, the bilayer is in the l_d phase, while (v) and (vi) shows that for $x > 10\%$, the membrane is at l_o-l_d coexistence. The phase transition for the symmetric bilayer is clearly at (iv) $x_c = 10\%$.

II. METHODS

A. Model membrane

We study the phase segregation and bilayer registry of a symmetric and asymmetric 3-component bilayer membrane embedded in an aqueous medium by atomistic molecular dynamics simulations using *GROMACS*. We prepare the bilayer membrane at 23 °C at different relative concentrations of palmitoyl-oleoyl-phosphatidyl-choline (POPC), long chain palmitoyl-sphingomyelin (SM-16:0) (PSM), and cholesterol (Chol). All multicomponent bilayer membranes have 512 lipids in each leaflet (with a total 1024 lipids) and 32 768 water molecules (such that the ratio of water to lipid is 32:1) so as to completely hydrate the simulated lipid bilayer.

For the symmetric bilayer, the relative concentration (in percentage, x) of PSM and Chol in the upper and lower leaflet is varied from $x\,(\text{in}\,\%) = 33.3\%, 19.9\%, 12.5\%, 10.0\%, 9.1\%, 7.1\%, 5.8\%, 2\%$, and 1%, with POPC contributing to the rest of the lipid content.

For the asymmetric bilayer, the upper leaflet has POPC /PSM /Chol in the ratio 1 : 1 : 1 (i.e., the relative concentration of each component is 33%). We vary the relative composition in the lower leaflet; denoting x as the relative concentration (in percentage) of PSM and Chol in the lower leaflet, we run through the values $x\,(\text{in}\,\%) = 33.3\%, 25.0\%, 19.9\%, 14.3\%, 12.5\%, 10.0\%, 9.1\%, 7.1\%, 5.9\%$, and 4.5%, with POPC contributing to the rest of the lipid content. With this choice of compositions and temperature, the upper leaflet is in the putative l_o-l_d phase coexistence regime (see Fig. 1(a), for the ternary phase diagram at 23 °C, taken from Ref. 28), while in the lower leaflet the compositions straddle the phase boundary allowing us to go from the l_o-l_d phase coexistence regime to the l_d phase, Fig. 2(a).

To study the role of lipid chemistry, we repeat the above set of simulations with PSM in the lower leaflet replaced by the short chain sphingomyelin, SM-14:0 (MSM). We vary the concentration x of MSM (Chol) across the range $x\,(\text{in}\,\%) = 4.5\%, 5.9\%, 7.1\%, 9.1\%, 10.0\%, 12.5\%$, and 14.35%.

B. Force fields

The force field parameters for POPC, PSM, and Chol are taken from the previous validated united-atom description

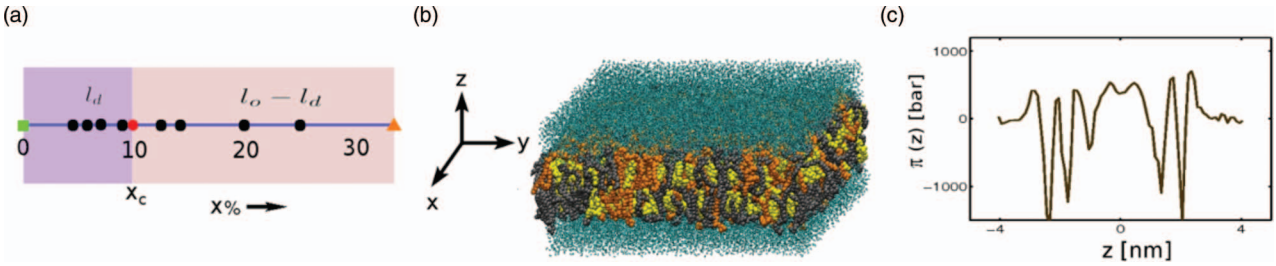

FIG. 2. (a) For the simulations of the asymmetric bilayer, we hold the composition of the upper leaflet at 1 : 1 : 1, while in the lower leaflet the composition of PSM and Chol is varied from $x = 33.3\%$ (orange dot) to 0% (green square), with POPC contributing to the rest. The composition where the simulations are carried out, denoted by black dots (see Sec. II), is indicated against the reference ternary phase diagram of the symmetric bilayer (blue line in Fig. 1(a)). Triangle (orange) represents the composition 1 : 1 : 1 which is deep in the phase coexistence region; for reference, dot (red) indicates the point on the phase boundary of the symmetric bilayer, $x_c = 10\%$. (b) Snapshot of equilibrium configuration of the asymmetric bilayer when $x = 25\%$, with POPC (gray), PSM (orange), Chol (yellow), and water (cyan). (c) Lateral pressure profile $\pi(z)$ for the same bilayer at equilibrium.

used the GROMOS force-field.[19–21] We construct the force field parameters for MSM (SM-14:0) from the parameters of PSM and POPC. We use the improved extended simple point charge (SPC/E) model to simulate water molecules, having an extra average polarization correction to the potential energy function.

C. Initial configurations

We generate the initial configurations of the asymmetric multicomponent bilayer membrane using *PACKMOL*.[22] For all simulation runs, we choose two sets of initial conditions: (i) where the components in each leaflet are homogeneously mixed and (ii) where the ternary components are completely phase segregated in l_o-l_d domains.[19]

D. Choice of ensembles and equilibration

The asymmetric bilayers are equilibrated for 50 ps in the NVT ensemble using a Langevin thermostat to avoid bad contacts arising from steric constraints and then for 160 ns in the NPT ensemble ($T = 296$ K (23 °C), $P = 1$ atm). The simulations are carried out in the NPT ensemble for the first 20 ns using Berendsen thermostat and barostat, then for 20 ns using Nose-Hoover thermostat and the Parrinello-Rahman barostat to produce the correct ensemble. Rest of the simulations are performed in the NPT ensemble using Berendsen thermostat. We use a semi-isotropic pressure coupling with compressibility 4.5×10^{-5} bar^{-1} for the simulations in the NPT ensemble.

The long-range electrostatic interactions are incorporated by the reaction-field method with cut-off $r_c = 2$ nm, while for the Lennard-Jones interactions we use a cut-off of 1 nm.[19,21,23] We have been able to reproduce earlier results on single and multi-component symmetric bilayer systems,[21,23] and so we are confident that these methods do not introduce artifacts in our simulations.

For each initial configuration, we run the simulations for 200 ns before computing the desired physical quantities. We calculate the lateral pressure profiles in the bilayer using Irving-Kirkwood contour and grid size 0.1 nm. We calculate the pairwise forces by rerunning the trajectory with cut-off 2 nm for electrostatic interactions using LINCS algorithm to constrain the bond lengths[24] and the SETTLE algorithm to keep the water molecules rigid[25] so that integrator time step of 2 fs can be used. We generate pressure profiles from trajectories over 20 ns using SHAKE algorithm[26] to constrain bond lengths.

E. Computation of deuterium order parameter

We calculate the spatial distribution of the deuterium order parameter S from the selected carbon atoms ($C5 - C7$) of each acyl chain (including SN1 and SN2 chains) of the PSM and POPC lipids.[19,21] Here, S is defined for every selected CH_2 group in the chains as, $S \equiv \frac{1}{2}\langle 3\cos^2\theta - 1\rangle$ where θ is the angle between a CH-bond and the normal to the plane of the membrane (z-axis). This is then coarse-grained (binned) over a spatial scale of 0.5 nm for last 20 ns of the trajectory of the simulations. We use our previous estimation of the deuterium order parameter S of the l_o-l_d domains of the bilayer membrane,[19] to declare a region to be liquid-ordered (l_o) when the value of $S \geq 0.35$.

F. Computation of mismatch area

We calculate the coarse-grained spatial profile of the deuterium order parameter S in each leaflet using grid size 0.5 nm. We then use the above cutoff in S to declare a region as liquid ordered. We compute the area and perimeter of the l_o domains in each leaflet using the cluster algorithm available in Image Processing Toolbox, MATLAB 2009. This is used to calculate the overlap and mismatch area of the domains across the bilayer (see, Sec. III D).

III. RESULTS AND DISCUSSION

A. Equilibrating the membrane

We rigorously ensure that the prepared bilayer membrane is mechanically stable, with both the net force and torque balanced. The forces, torques, and surface tension of the bilayer are computed from the local stress tensor, which in turn is calculated through the virial, $\sigma_{ij}(x, y, z) = \frac{1}{v}\sum_\alpha f_i^\alpha r_j^\alpha$, where f_i^α is the ith component of the force on the αth-particle due to all other particles within a coarse-grained volume $v = [0.1\,\text{nm}]^3$. We compute the net force

$$F_i = \int \partial_k \sigma_{ik}\, dv \tag{1}$$

and net torque

$$M_{ik} = \int (\partial_l \sigma_{il} x_k - \partial_l \sigma_{kl} x_i)\, dv \tag{2}$$

of the bilayer and find both force and torque balance at late times, $t > 150$ ns in our simulation runs. The time series of the components of the force and torque show that their local mean values and fluctuations decrease as time progresses, till at times $t > 150$ ns, they approach zero with small fluctuations about it (see Figures S1 and S2 in the supplementary material).[31] The mean values with error bars at late times are comparable to the corresponding values for the symmetric one-component bilayer membrane.[19] This shows that we obtain a mechanically stable asymmetric bilayer at late times. In addition we ensure that the surface tension at late times is zero to within numerical error. The membrane surface tension is calculated as

$$\gamma = \int \pi(z) dz, \tag{3}$$

integrated over the width of the bilayer, where $\pi(z)$ is the lateral pressure, given by[23,27]

$$\pi(z) = \frac{1}{2}(\overline{\sigma}_{xx}(z) + \overline{\sigma}_{yy}(z)) - \overline{\sigma}_{zz}(z); \tag{4}$$

the time series of γ is seen to approach zero (with small fluctuations about it), showing that we obtain a "tensionless" bilayer at late times (see Figures S3 and S4 in the supplementary material).[31]

We ensure that the bilayer membrane approaches and attains thermodynamic equilibrium, by monitoring the energy (data not shown) and area per lipid, and the mean deuterium order parameter S, throughout the simulations (see Figures S5-S8 in the supplementary material).[31] These quantities settle to a constant value at late times, $t > 150$ ns in our simulation runs, with small fluctuations about it.

It might appear that $t \approx 200$ ns do not constitute very late times in our simulation runs, and so how can we be sure that we have attained equilibrium. By using a judicious choice of initial conditions, we have made sure that the system has *either reached equilibrium or is approaching equilibrium*. We have verified this approach to equilibrium by monitoring the time series of a variety of thermodynamic, mechanical and chemical quantities, as listed above. As mentioned in *Materials and Methods*, the simulations have been carried out from two sets of initial conditions. One set of initial conditions is where the composition is *homogeneously mixed* in each leaflet, while the other set of initial conditions is where the composition is completely segregated. The choice of initial condition is dictated by how fast we attain equilibration. Thus if the equilibrium configuration is expected to show l_o-l_d phase coexistence, then the preferred initial condition is a fully segregated bilayer, with minimal interfacial boundary. If however the equilibrium configuration is expected be in the l_d-phase, then the preferred initial condition is a homogenous mixed configuration. For the asymmetric bilayer, the initial configuration of the upper leaflet is taken from the final equilibrium configuration of a symmetric ternary component bilayer at 200 ns.

Figure 1(a) shows the ternary phase diagram of the symmetric bilayer comprising POPC, PSM (long chain palmitoylsphingomyelin, SM-16:0), and Chol at 23 °C taken from an earlier study.[28] We have ourselves simulated the symmetric bilayer membrane composed of POPC, PSM, and Chol with concentration, $x = 1\%, 2\%, 5.8\%, 7.1\%, 9.1\%, 10\%, 12.5\%, 19.9\%$, and 33.3% of the PSM (Chol). To determine the phase diagram, we have computed $P(\phi)$, the distribution of the order parameter $\phi = \frac{\rho_{PSM}-\rho_{POPC}}{\rho_{PSM}+\rho_{POPC}}$, at different values of x (Fig. 1(b)). This clearly shows that phase transition from the l_d-phase to the l_o-l_d phase coexistence regime occurs at $x_c = 10\%$.

Our results for the symmetric bilayer are therefore consistent with earlier studies.[28]

We perform simulations on our model asymmetric bilayer at varying concentrations x of PSM and Chol in the lower leaflet, whilst maintaining the upper leaflet at a composition 1 : 1 : 1, which is deep in the l_o-l_d phase coexistence region. The simulations done at various values of x along the line shown in Fig. 2(a), traverse across the phase boundary at $x_c = 10\%$ into the l_d phase.

Here, we show an equilibrium snapshot of the ternary asymmetric bilayer membrane composed of POPC, PSM, and Chol and its lateral pressure profile $\pi(z)$, Figs. 2(b) and 2(c), respectively (equilibrium pressure profiles at other concentrations are displayed in Figures S9 and S10 in the supplementary material).[31]

We perform a similar study when the lower leaflet PSM is replaced by MSM (the short chain sphingomyelin, SM-14:0).

B. Lateral compositional heterogeneity

The coarse-grained spatial profile of the lipid number density is calculated with a grid size 1.3 nm. As stated in Sec. II, the composition in the upper leaflet is fixed at 1 : 1 : 1, while the composition of PSM/Chol in the lower leaflet is varied from 33% to 4.5%. The top and middle panels in Fig. 3 show the spatial profile of the number density of PSM in the upper and lower leaflets, respectively, at 4 representative compositions on either side of the phase boundary, $x_c = 10\%$. The lower panel, described in Sec. III C, shows the joint correlation of the PSM rich domains across the bilayer.

Figure 4 shows a similar study done when PSM in the lower leaflet is replaced by short chain MSM.

C. Domain registry across bilayer

We have studied the extent of registry of l_o-l_d domains across the bilayer of an asymmetric multicomponent membrane as a function of varying composition and lipid chemistry. We measure the extent of transbilayer registry by computing the joint probability distribution (JPD) of the coarse-grained number density of PSM in the upper and lower leaflets at the same coarse-grained spatial location (x, y). The lower panel of Fig. 3 shows the JPD at different values of the concentration x of PSM in the lower leaflet.

In the lower panel in Fig. 3, the JPD shows a distinct peak along the diagonal when $x > x_c = 10\%$, which is clear evidence of *bilayer registry* of l_o-domains. The off-diagonal peak in the JPD is merely an indication of the relative abundance of PSM in the upper leaflet. On the other hand, for $x \ll x_c$, this diagonal peak in the JPD is absent, indicating lack of bilayer registry.

A similar conclusion regarding the bilayer registry can be drawn when the lower leaflet PSM is replaced by the short chain MSM (Fig. 4).

These observations suggest that the configurations of the two leaflets mutually influence each other. As stated in the *Abstract*, we can ask whether the segregation of lipids in the upper leaflet can induce a phase segregation in lower leaflet, i.e., can the composition in the upper leaflet act as a local "field" for the composition in the lower leaflet. To study this, we define a "transbilayer correlation coefficient" from the normalized transbilayer correlation (r denotes the 2d coordinate (x, y)),

$$C\left(\rho^u_{PSM}(r), \rho^l_{PSM}(r)\right) = \frac{\left\langle \rho^u_{PSM}(r)\rho^l_{PSM}(r)\right\rangle - \left\langle \rho^u_{PSM}(r)\right\rangle\left\langle \rho^l_{PSM}(r)\right\rangle}{\sqrt{\left\langle \rho^u_{PSM}(r)^2\right\rangle - \left\langle \rho^u_{PSM}(r)\right\rangle^2}\sqrt{\left\langle \rho^l_{PSM}(r)^2\right\rangle - \left\langle \rho^l_{PSM}(r)\right\rangle^2}}, \tag{5}$$

averaged over space (denoted by C_{ul}) and compute this as a function of the relative concentration x of PSM/Chol. Note that each quantity in the transbilayer correlation is of the form $\langle A(r)B(r)\rangle - \langle A(r)\rangle\langle B(r)\rangle$, and is nonzero if and only if A and B are correlated. Figure S11 in the supplementary material shows the transbilayer correlation coefficient C_{ul} as a function of x for a symmetric bilayer.[31] C_{ul} jumps from a high

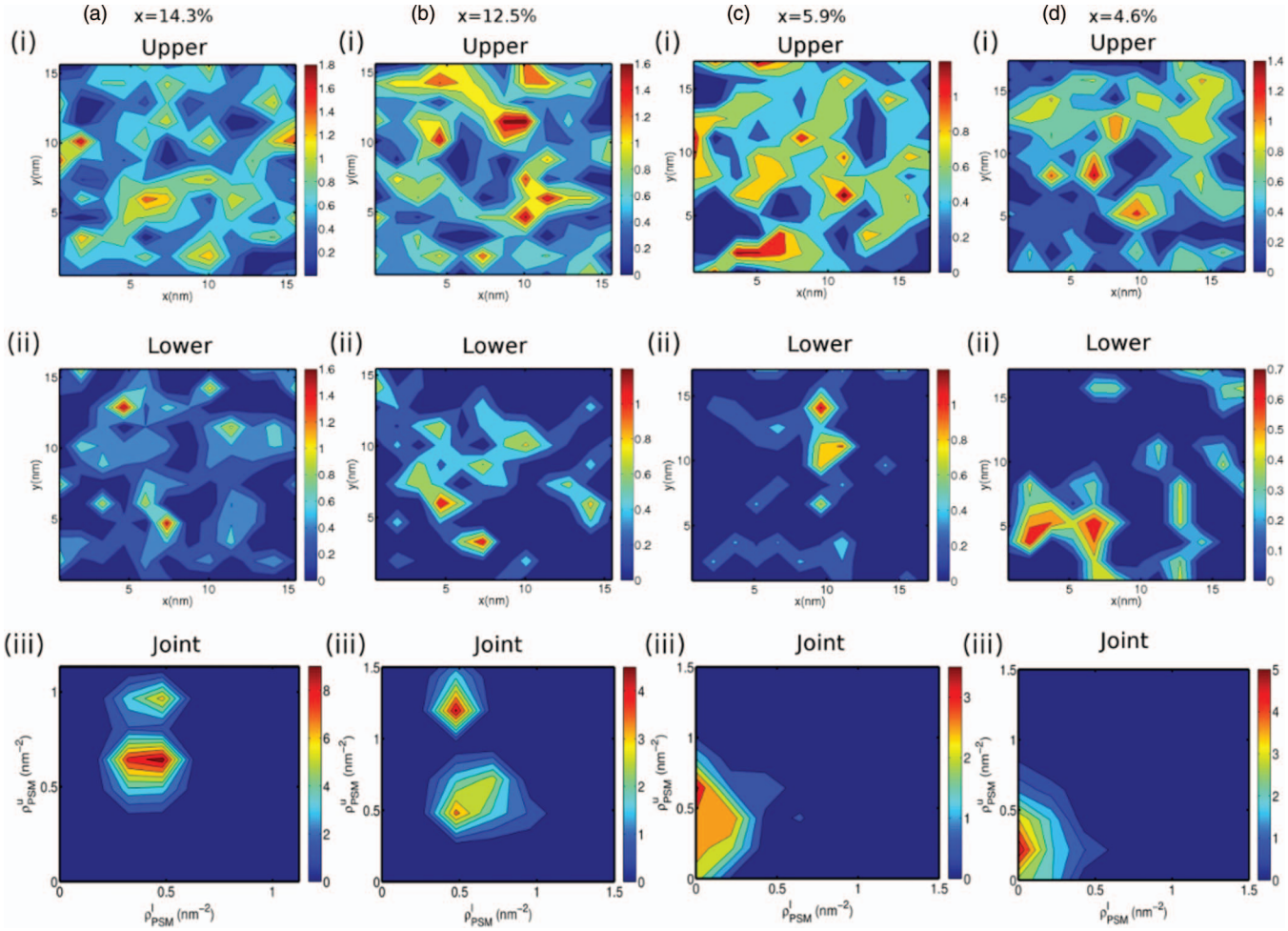

FIG. 3. Spatial profile of the coarse-grained number density of PSM (color bar) in the upper leaflet (top panel) at different compositions of PSM in the lower leaflet (as indicated at the top of the panels). The middle panel shows the corresponding profile of the number density of PSM (color bar) in the lower leaflet. The bottom panel shows the extent of correlation between the PSM-rich domains across the bilayer, as measured by the joint probability distribution, JPD (color bar, see text). For $x > x_c = 10\%$, the JPD shows strong transbilayer correlations, while for $x \ll x_c$, the correlations are poor. The exact value of x at which this crossover occurs is estimated in Fig. 5.

value in the $l_o - l_d$ phase coexistence region to a low value in the l_d phase. The jump in C_{ul} coincides with the phase boundary $x_c = 10\%$ (Fig. 1).

For the asymmetric bilayer, we compute the transbilayer correlation coefficient as a function of x, the concentration of PSM (or MSM) in the lower leaflet (Fig. 5). The transbilayer correlation coefficient C_{ul} is very nearly zero for $x \ll x_c$ and rises sharply to $\sim$1 at $x = x_c^{PSM} < x_c$, showing the influence of the upper leaflet on the phase segregation of the lower. This transbilayer influence is stronger for the long chain PSM than for the short chain MSM, as seen by the fact that $x_c^{MSM} = 9.09\% > x_c^{PSM} = 5.88\%$.

There is thus a shift in the phase boundary from its value of $x_c = 10\%$ for the ternary symmetric bilayer of POPC-PSM-Chol. This shift is plotted as $\Delta = |x_c^{PSM/MSM} - x_c|$ for both the long chain PSM ($\Delta^{PSM} = 4.12\%$) and short chain MSM ($\Delta^{MSM} = 0.91\%$) in the lower leaflet (inset Fig. 5).

The above phenomenology can be understood within a mean-field theory of phase transitions,[29] with a Helmholtz free-energy functional written in terms of ϕ_u and ϕ_l, where ϕ_u (ϕ_d) is the relative concentration of the l_o and l_d species in the upper (lower) leaflet. The form of the free-energy functional for the asymmetric bilayer can be written as,

$$F[\phi_u, \phi_l] = \frac{1}{2}\int d^2x\,[f_u(\phi_u) + f_l(\phi_l) + f_{ul}(\phi_u, \phi_l)]$$

$$f_u = C_u(\nabla\phi_u)^2 - r_u\phi_u^2 + u\phi_u^3 + v\phi_u^4$$

$$f_l = C_l(\nabla\phi_l)^2 + r_l\phi_l^2$$

$$f_{ul} = -A\phi_u\phi_l + B\phi_u\phi_l^2 + D\phi_u^2\phi_l, \qquad (6)$$

where $r_u \sim (x - x_c^u)$, $r_l \sim (x - x_c^l) > 0$ reflects the fact that the upper leaflet is in the l_o-l_d phase coexistence regime, $\langle\phi_u\rangle \neq 0$, and the isolated lower leaflet is in the l_d phase, $\langle\phi_l\rangle = 0$. The coefficient $A > 0$ to account for the fact that the local transbilayer coupling is attractive.

We first minimize F with respect to ϕ_u:setting $\delta F/\delta\phi_u = 0$, and keeping terms to linear order, we get

$$C_u\nabla^2\phi_u + r_u\phi_u = A\phi_l\,, \qquad (7)$$

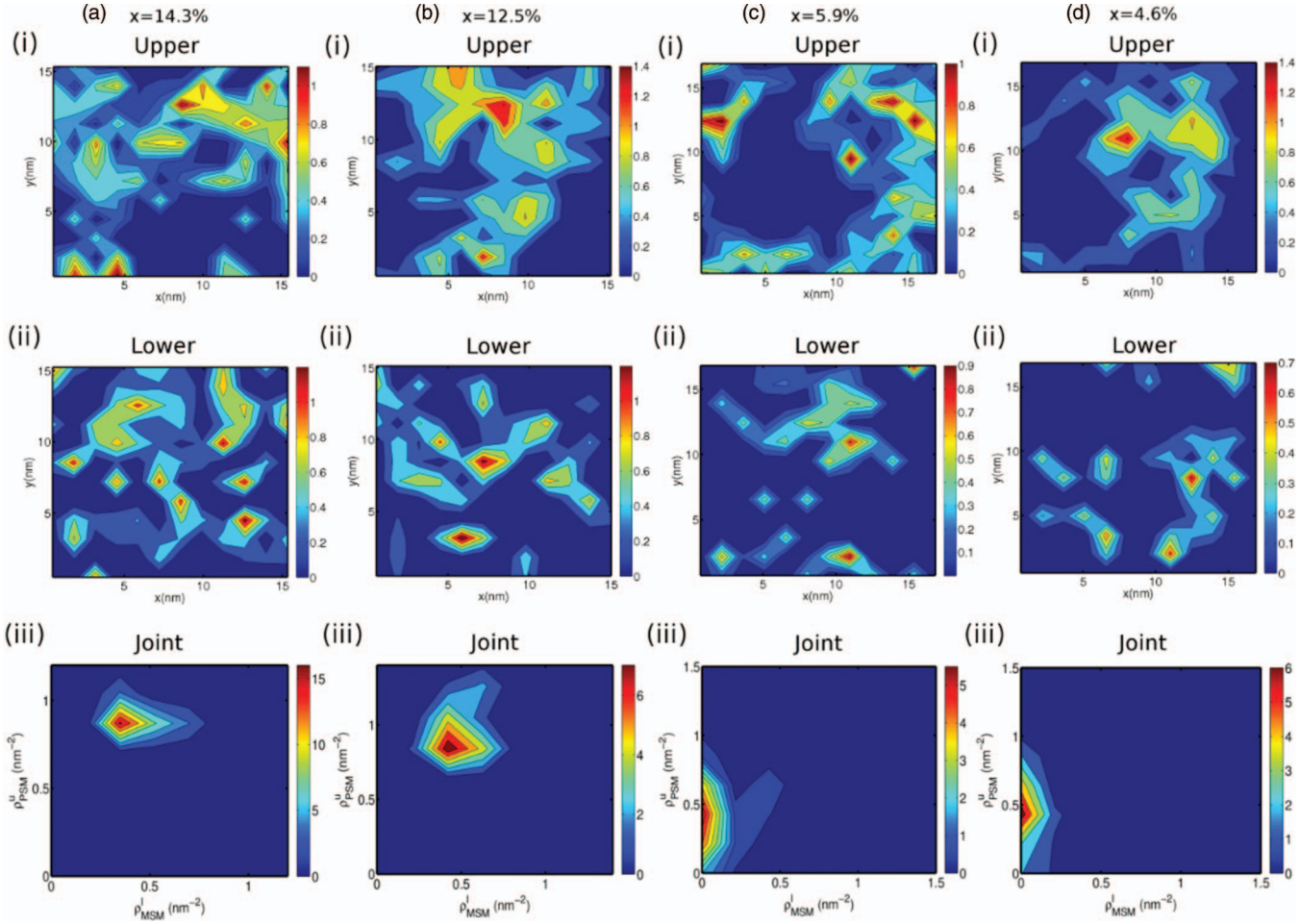

FIG. 4. Spatial profile of the coarse-grained number density of PSM (color bar) in the upper leaflet (top panel) at different compositions of MSM in the lower leaflet (as indicated at the top of the panels). The middle panel shows the corresponding profile of the number density of MSM (color bar) in the lower leaflet. The bottom panel shows the extent of correlation between the PSM-rich domain in the upper leaflet and the MSM-rich domain in the lower leaflet, as measured by the joint probability distribution, JPD (color bar, see text). As in Fig. 3, for $x > x_c = 10\%$, the JPD shows strong transbilayer correlations, while for $x \ll x_c$, the correlations are poor. The exact value of x at which this crossover occurs is estimated in Fig. 5.

whose Fourier transform, lends itself to a useful interpretation,

$$\phi_u(\mathbf{q}) = \frac{A\phi_l(\mathbf{q})}{-C_u q^2 + r_u}, \tag{8}$$

namely, a spatially varying ϕ_u can induce a spatially varying ϕ_l. Nonlinearities in the free-energy that we have neglected, reinforce this and will lead to bilayer registry. Plugging this expression back into Eq. (3), we obtain an effective free-energy functional in terms of ϕ_l alone, which shows that the coefficient of the quadratic term gets reduced by $r_l \to r_l - A^2/r_u$, which for large enough A can become negative. This shows that the segregation in the upper leaflet can induce a segregation in the lower, by shifting the phase transition point. This mean field analysis is entirely consistent with our MD simulations.

D. Mismatch area and interfacial tension

When there is perfect bilayer registry, the area of the l_o domain in the upper leaflet will completely overlap with the area in the lower leaflet (Fig. 6(a)). Any mismatch in the overlap area will cost energy proportional to the mismatch area A, defined as $A = A^u_{l_o} + A^l_{l_o} - 2A^o$, where $A^u_{l_o}$ and $A^l_{l_o}$ are the areas of the l_o-domains in the upper and lower leaflets and A^o is the overlap area between the l_o-domains in the upper and lower leaflets (Fig. 6(b)). The proportionality constant is a tension γ or a mismatch free energy per unit area, and is a measure of the domain overlap, a larger value of γ implies a more complete overlap. This tension γ acts as a driving force for inter-leaflet registration of the phase domains across the bilayer. In principle, the value of the tension γ is affected by short wavelength curvature and protrusion fluctuations, which we have ignored in our computation of the area—this will typically go to reduce the value of γ.

The linear dependence of the energy on the mismatch area A holds as long as the mean size of the mismatch region $\langle R \rangle$ is larger than its root mean square fluctuation $w = \sqrt{\langle \delta R^2 \rangle}$, where $\delta R = R(\theta) - \langle R \rangle$, and $R(\theta)$ is the distance from the domain centre to the domain boundary at the angular position θ. There are strong corrections to this leading behaviour, of order $(w/\langle R \rangle)^2$, when the domains are small or ramified. Given that the lateral dimension of the model membrane is 15.6 nm, this is likely the case in our atomistic MD

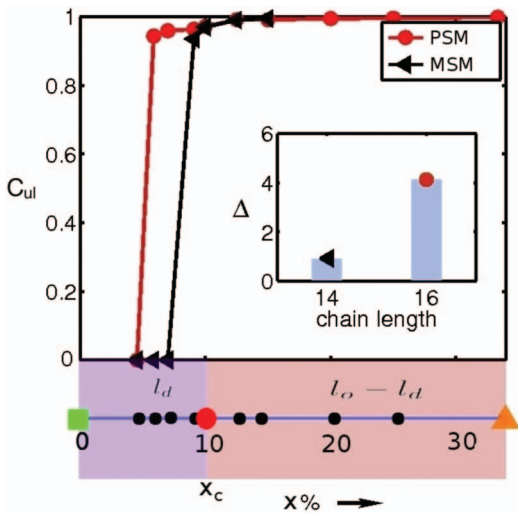

FIG. 5. Transbilayer correlation coefficient C_{ul} defined from the transbilayer correlation $C(\rho^u(r), \rho^l(r))$ (see text) between the density of upper leaflet PSM and lower leaflet PSM (red circle) or MSM (black triangle) versus x, the concentration of PSM or MSM in the lower leaflet. Color panel below drawn for reference denotes the values of x at which C_{ul} has been evaluated. The value of C_{ul} is zero for small x and jumps sharply at $x_c^{PSM/MSM} < x_c = 10\%$ (red dot in color panel), indicating a first-order phase transition. The phase transition point for the long chained PSM, $x_c^{PSM} = 5.88\%$ is smaller than that of the short chained MSM $x_c^{MSM} = 9.09\%$. Inset shows the shift in the transition Δ (see text) as a function of lipid chain length.

simulations. To check this, we have plotted the perimeter per area of the mismatch region (see Figure S12 in the supplementary material)[31] versus area at different values of x, the relative concentration of PSM in the lower leaflet—this shows that the mean domain shapes deviate from circularity, especially for small values of x.

With this caveat, we have estimated the domain interfacial tension γ by computing the probability distribution of the mismatch area A of the l_o-domains between the two leaflets of the bilayer, and equating it to the Boltzmann form, $P(A) \propto \exp(-\gamma A)$, where γ is measured in units of $k_B T$. In Figure S13 of the supplementary material,[31] the plot of the probability distribution of A at various values of x shows a distinct peak at the most probable value of A; in a semi-log plot Fig. 6(c), we fit the distribution to the Boltzmann form to extract the value of the tension γ. The values of γ obtained here at values of x well within the coexistence region—for instance $\gamma = 0.146 \pm 0.02\ \mathrm{k_B T/nm^2}$ at $x = 33\%$—are consistent with those obtained from other coarse-grained simulations.[11,30] Given the systematic errors in such a computation and the caveats mentioned above, we should regard this computed value of γ with some caution. Notwithstanding, the qualitative trend showing γ decrease with x, with a sharp drop to zero at $x \simeq x_c^{PSM}$ (Fig. 6(d)), is reassuring—indeed γ goes to zero at precisely $x_c = 10\%$ for the symmetric bilayer.

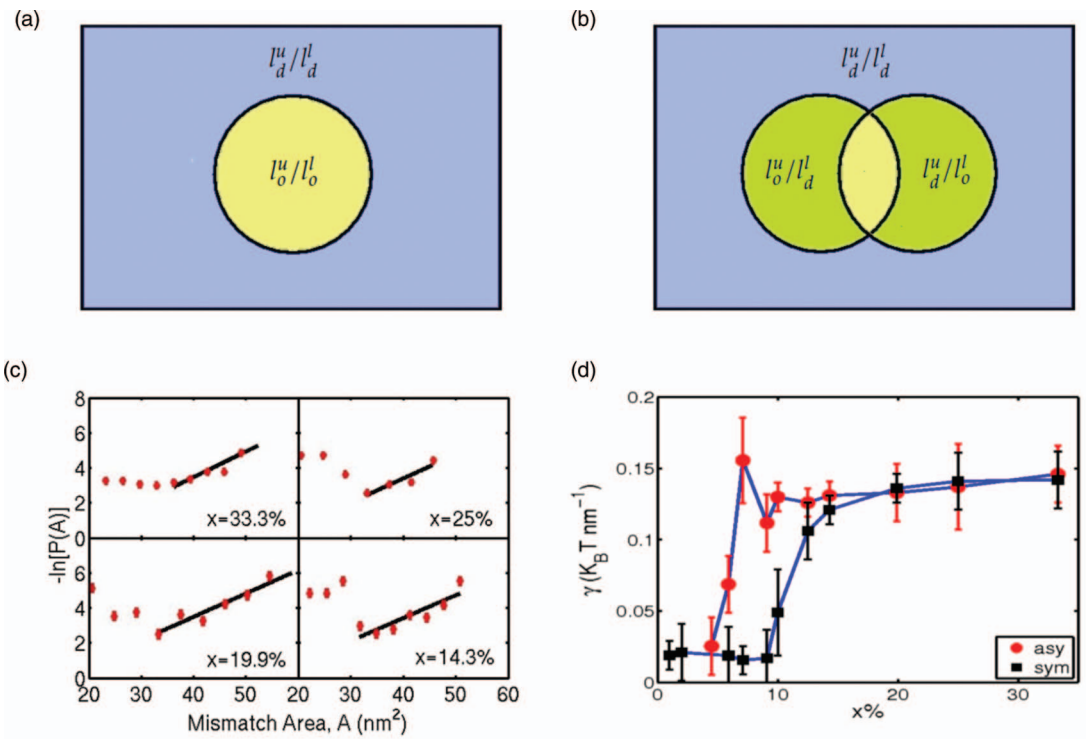

FIG. 6. Schematic showing (a) domains in complete registry or overlap across the bilayer and (b) domains in partial overlap with a defined mismatch area (see text). (c) Semi-log plot of the probability distribution of the mismatch area, $-\ln P(A)$ vs. A (red dots), at different values of x, the concentration of PSM in the lower leaflet (indicated in the panel). The straight lines in the high A regime are fits to the Boltzmann form (see text), from which we extract the value of the tension γ. Error bars are indicated. (d) Tension γ as a function of x (red dots) shows a sharp drop to zero at $x \simeq x_c^{PSM}$. In comparison, for the symmetric bilayer, γ drops sharply to 0 at precisely $x_c = 10\%$ (black squares).

IV. CONCLUSION

We have analyzed the equilibrium properties of a ternary component, asymmetric bilayer membrane using atomistic molecular dynamics study. Our central goal was to study the conditions under which bilayer registry takes place in an asymmetric, multicomponent membrane. To summarize, our main results are: (i) l_o phase domains formed in the two leaflets are registered across the bilayer membrane, (ii) phase segregation in upper leaflet can induce segregation in the lower, thus the composition on the upper leaflet acts as a "field" which couples linearly to the composition in the lower leaflet, and (iii) the strength of the transbilayer coupling and the extent of bilayer registry depends sensitively on the lipid chain length and is greater for longer chain lipids.

The registry of the phase domains across the two leaflets of the bilayer membrane has an important implication to the sorting and signaling in live cell membrane. The cell membrane is inherently asymmetric with both lateral and transverse lipid heterogeneity. Recent experiments on live cells, using FRET,[16–18] show that outer leaflet GPI-APs organized as monomers and cholesterol-sensitive nanoclusters are regulated by the active dynamics of cortical actin (CA) and myosin. The present work forms the basis for further investigation of the transbilayer interaction between lateral heterogeneities of the outer leaflet GPI-anchored proteins, PSM, and cholesterol with saturated, long chain lipids at the inner leaflet whose organization depends on the actin and actin remodeling proteins.

ACKNOWLEDGMENTS

S.M. is a J. C. Bose Fellow (DST, Government of India) and acknowledges support from an HFSP grant. This work was partially supported by a grant from Simons Foundation.

[1]K. Simons and E. Ikonen, Nature (London) **387**, 569–572 (1997).
[2]D. Lingwood and K. Simons, Science **327**, 46–50 (2010).
[3]K. Simons and D. Toomre, Nat. Rev. Mol. Cell. Biol. **1**, 31–39 (2000).
[4]S. Mayor and M. Rao, Traffic **5**, 231–240 (2004).
[5]S. L. Veatch and S. L. Keller, Phys. Rev. Lett. **89**, 268101 (2002).
[6]S. L. Veatch and S. L. Keller, Biophys. J. **85**, 3074–3083 (2003).
[7]T. Baumgart, S. Hess, and W. Webb, Nature (London) **425**, 821–824 (2003).
[8]C. Wan, V. Kiessling, and L. Tamm, Biochemistry **47**, 2190–2198 (2008).
[9]M. Collins and S. Keller, Proc. Natl. Acad. Sci. U.S.A. **105**, 124–128 (2008).
[10]D. W. Allender and M. Schick, Biophys. J. **91**, 2928–2935 (2006).
[11]G. Putzel, M. Uline, I. Szleifer, and M. Schick, Biophys. J. **100**, 996–1004 (2011).
[12]H. Risselada and S. Marrink, Proc. Natl. Acad. Sci. U.S.A. **105**, 17367–17372 (2008).
[13]A. Kusumi, I. Koyama-Honda, and K. Suzuki, Traffic **5**, 213–230 (2004).
[14]S. I. Hakomori, Biochim. Biophys. Acta **1780**, 325–346 (2008).
[15]J. F. Hancock, Nat. Rev. Mol. Cell Biol. **7**, 456–462 (2006).
[16]P. Sharma, R. Varma, R. Sarasij, Ira, K. Gousset, G. Krishnamoorthy, M. Rao, and S. Mayor, Cell **116**, 577–589 (2004).
[17]D. Goswami, K. Gowrishankar, S. Bilgrami, S. Ghosh,R. Raghupathy, R. Chadda, R. Vishwakarma, M. Rao, and S. Mayor, Cell **135**, 1085–1097 (2008).
[18]K. Gowrishankar, S. Ghosh, S. Saha, C. Rumamol, S. Mayor, and M. Rao, Cell **149**, 1353–1367 (2012).
[19]A. Polley, S. Vemparala, and M. Rao, J. Phys. Chem. B **116**, 13403–13410 (2012).
[20]D. P. Tieleman and H. J. Berendsen, Biophys. J. **74**, 2786–2801 (1998).
[21]P. S. Niemelä, S. Ollila, M. T. Hyvönen, M. Karttunen, and I. Vattulainen, PLoS Comput. Biol. **3**, e34 (2007).
[22]L. Martínez, R. Andrade, E. Birgin, and J. Martínez, J. Comput. Chem. **30**, 2157–2164 (2009).
[23]M. Patra and M. Karttunen, J. Phys. Chem. B **108**, 4485–4494 (2004).
[24]B. Hess, H. Bekker, H. J. C. Berendsen, and J. G. E. M. Fraaije, J. Comput. Chem. **18**, 1463–1472 (1997).
[25]S. Miyamoto and P. A. Kollman, J. Comput. Chem. **13**, 952–962 (1992).
[26]J.-P. Ryckaert, G. Ciccotti, and H. J. Berendsen, J. Comput. Phys. **23**, 327–341 (1977).
[27]S. A. Safran, *Statistical Thermodynamics of Surfaces, Interfaces, and Membranes* (Addison-Wesley, 1994).
[28]R. F. M. de Almeida, A. Fedorov, and M. Prieto, Biophys. J. **85**, 2406–2416 (2003).
[29]P. M. Chaikin and T. C. Lubensky, *Principles of Condensed Matter Physics* (Cambridge University Press, 2000).
[30]E. B. Watkins, C. E. Miller, J. Majewski, and T. L. Kuhl, Proc. Natl. Acad. Sci. U.S.A. **108**, 6975–6980 (2011).
[31]See supplementary material at http://dx.doi.org/10.1063/1.4892087 for time series of force, torque, surface tension, area per lipid, and deuterium order parameter of the mechanically stable asymmetric multicomponent lipid bilayers. In addition, figures describing additional details of the equilibrium pressure, transbilayer correlation coefficient, ratio of the perimeter to area of the mismatch area, and probability of mismatch area of the various model systems have been included.